

## Experimental kinematics for wheeled skid-steer mobile robots

Anthony Madow, Jorge L. Martínez, Jesús Morales, José L. Blanco,

Alfonso García-Cerezo and Javier González

Dpto. Ingeniería de Sistemas y Automática, Universidad de Málaga, 29013 Málaga, Spain

Email: amadow@uma.es, Tel: (+34) 952 131407, Fax: (+34) 952 131413

**Abstract**—This work aims at improving real-time motion control and dead-reckoning of wheeled skid-steer vehicles by considering the effects of slippage, but without introducing the complexity of dynamics computations in the loop. This traction scheme is found both in many off-the-shelf mobile robots due to its mechanical simplicity and in outdoor applications due to its maneuverability. In previous works, we reported a method to experimentally obtain an optimized kinematic model for skid-steer tracked vehicles based on the boundedness of the Instantaneous Centers of Rotation (ICRs) of treads on the motion plane. This paper provides further insight on this method, which is now proposed for wheeled skid-steer vehicles. It has been successfully applied to a popular research robotic platform, Pioneer 3-AT, with different kinds of tires and terrain types.

### I. INTRODUCTION

Wheeled skid-steering drive mechanisms are found in many all-terrain vehicles, such as loaders, farm machinery, mining and military. This traction scheme is also useful for off-road mobile robots [1], with field applications such as planetary exploration [2], land-mine detection [3] and rescue [4]. Moreover, commercial robotic research platforms also employ this locomotion system [5].

Steering is based on controlling the relative velocities of the left and right side drives, similarly to differential drive wheeled vehicles. However, since all wheels are aligned with the longitudinal axis of the vehicle, turning requires wheel slippage. This locomotion system functions like that of a tracked vehicle. Tracked locomotion usually provides better traction, but it is mechanically more complex [6].

Wheeled skid-steering presents two major advantages over alternative wheel configurations, such as Ackerman or axle-articulated. First, it is simple and robust in mechanical terms. Second, it provides better manoeuvrability, including zero-radius turning, using only the components needed for straight-line motion [2].

However, this locomotion scheme poses special difficulties when addressing motion control and odometry. Skid-steering kinematics is not straightforward, since it is not possible to predict the exact motion of the vehicle only from its control inputs. Thus, pure rolling and no-slip assumptions considered in kinematic models for non-holonomic wheeled vehicles do not apply in this case.

Nevertheless, we find that scarce work has been reported on this problem. Additional internal sensor, such as gyroscopes [7], inertial units [8] or a small passive trailer with encoders [9] can be applied to detect heading changes that

are not sensed by the motor encoders. Still, an effective kinematic model is necessary to perform on-board computations for dead-reckoning and motion control in the short term.

Some authors have studied stability of wheeled skid-steering with non-linear control techniques by explicitly considering dynamics and drive models [10] [11]. Moreover, kinematics has been addressed in some works as the relation of linear and angular velocities with the position of the vehicle [12] [13]. However, these do not consider major skid effects, which arise at a lower level, in the relation between drive velocities and vehicle velocities.

A kinematic model that relates to identification of slip parameters from actual inertial readings was proposed in [14] for velocity control of tracked vehicles. For wheeled skid-steering, on-line adaptive control has been considered for estimation of tire/ground friction of a simplified dynamic model [15].

The kinematic relation is explicitly expressed by [8] as a terrain-dependent  $3 \times 2$  matrix of constant coefficients. This matrix does not only capture wheel skid but also tire pressure differences and transmission inaccuracies, although no physical meaning is given to its elements. A custom-made caster wheel trailer is used to measure the actual velocities in order to derive the coefficients with linear regression techniques.

Kinematic equivalences between skid-steering and differential drive vehicles have been proposed for tracked vehicles. A simple experiment to directly obtain a symmetric model was presented in [16]. Moreover, constant kinematic parameters are derived in [17] as optimized values for the Instantaneous Centers of Rotation (ICRs) of treads on the plane by using laser scan-matching motion estimations. These correspond to the position of ideal differential drive wheels for a particular terrain. This is based on the fact that positions of tread ICRs are dynamics-dependent, but they lie within a bounded area at moderate speeds. Kinematic identification also incorporates fine-tuning for misalignments and other mechanical inaccuracies.

This paper presents further work on the experimental ICR kinematic method, which is now proposed for wheeled skid-steer vehicles. It has been applied to Pioneer 3-AT, a commercial platform widely used as a test-bed for robotics research. For instance, a fuzzy path tracker [12] and independent control for each wheel to reduce odometry errors [18] have been reported.

The major contributions presented by this paper are the

following:

- A geometric interpretation of the kinematic matrix in [8] based on the geometric analogy with an ideal differential drive model.
- An easy to reproduce experimental identification method based on external sensor motion estimation and Genetic Algorithms to derive an approximate kinematic model for wheeled skid-steer vehicles.
- A kinematic analysis of the Pioneer P3-AT robot. Configuration parameters of the manufacturer's implicit kinematic model are related to the proposed method.
- Dead reckoning results obtained from the application of the experimental model with different wheel and terrain configurations.

Following this introduction, section 2 establishes kinematic analogies of skid-steering with ideal differential drive. Section 3 presents an experimental procedure for kinematics identification with external sensors. Section 4 describes the application to the P3-AT mobile robot as well as validation experiments. Section 5 is devoted to conclusions and ideas for future work. Finally, acknowledgements and references complete the paper.

## II. ANALOGY OF SKID-STEERING WITH DIFFERENTIAL DRIVE

Dynamic models for skid-steering may result too costly for real-time motion control and dead-reckoning. Alternatively, this section discusses geometric relationships that can be used instead.

When differential drive is applied to control a pair of pure rolling wheels, no slippage occurs and each tread's contact is limited to a single point. This assumption is usually adequate for non-ideal wheels with a relatively small contact patch (see Fig. 1.a). On the other hand, tracked vehicles with differential drive epitomize skid-steering because of the large contact area of both treads (see Fig 1.b). A similar case is represented by wheeled skid-steering, where each side's tread consists of several contact patches that correspond to mechanically linked wheels, as those within the dashed lines in Fig 1.c-d.

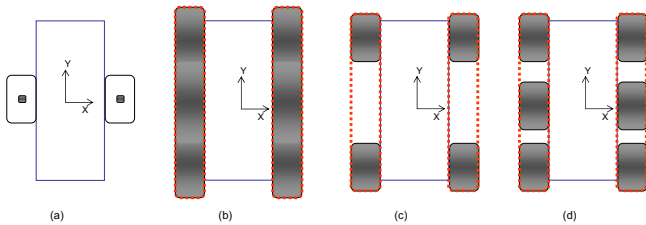


Fig. 1. Left and right treads on the plane for differential drive (a), tracked vehicle (b), four-wheel skid-steer vehicle (c), and six-wheel skid-steer vehicle (d).

The local frame of the vehicle is assumed to have its origin on the center of the area defined by the left and right contact surfaces on the plane, and its Y axis is aligned with the forward motion direction. Skid-steer vehicles are governed by two control inputs: the linear velocity of its left and right

treads with respect to the robot frame ( $V_l, V_r$ ). Then, direct kinematics on the plane can be stated as follows:

$$\begin{pmatrix} v_x \\ v_y \\ \omega_z \end{pmatrix} = f_d \begin{pmatrix} V_l \\ V_r \end{pmatrix} \quad (1)$$

where  $v = (v_x, v_y)$  is the vehicle's translational velocity with respect to its local frame, and  $\omega_z$  is its angular velocity.

When turning, the Instantaneous Center of Rotation (ICR) of the vehicle on the motion plane is expressed in local coordinates as  $ICR_v = (x_{ICRv}, y_{ICRv})$ , as shown in Fig. 2. Besides, the ICRs for the left and right treads can be defined in the local frame as  $ICR_l = (x_{ICRl}, y_{ICRl})$  and  $ICR_r = (x_{ICRr}, y_{ICRr})$ , respectively. These result from the composition of the motion of the vehicle and that of linear tread velocity (i.e.,  $V_l$  or  $V_r$ ). It is known [17] that  $ICR_l$  and  $ICR_r$  lie on a line parallel to the local X axis that also contains  $ICR_v$ . Note that treads have the same angular velocity  $\omega_z$  as the whole vehicle.

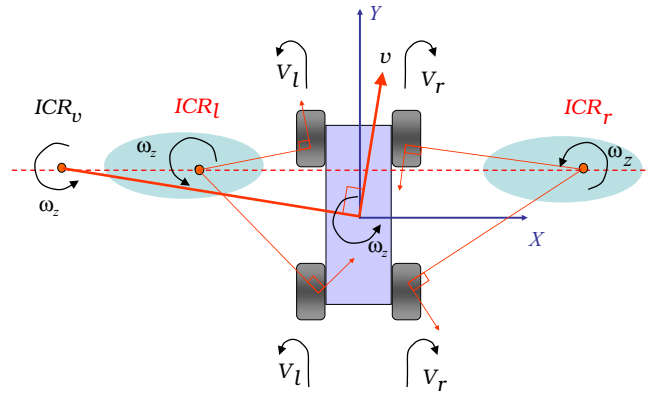


Fig. 2. Vehicle and tread ICRs on the plane.

Thus, the geometrical relation between ICR positions and the vehicle's translational and rotational velocities is expressed by:

$$x_{ICRv} = \frac{-v_y}{\omega_z} \quad (2)$$

$$x_{ICRl} = \frac{\alpha_l \cdot V_l - v_y}{\omega_z} \quad (3)$$

$$x_{ICRr} = \frac{\alpha_r \cdot V_r - v_y}{\omega_z} \quad (4)$$

$$y_{ICRv} = y_{ICRl} = y_{ICRr} = \frac{v_x}{\omega_z} \quad (5)$$

where the nominal tread speeds have been affected by correction factors ( $\alpha_l, \alpha_r$ ) to account for a number of fuzzy mechanical issues such as tire inflation conditions or the transmission belt tension.

The vehicle's  $x_{ICRv}$  coordinate reaches infinite values when  $\omega_z = 0$  in (2). Conversely, boundedness is an important property of tread ICR coordinates: In the proximity of straight line motion, numerators and denominators in (3)-(5) are infinitesimals of the same order, which result in finite values for  $x_{ICRl}$ ,  $x_{ICRr}$  and  $y_{ICRv}$ , respectively. It

must be noted that this boundedness is limited to the case of kinematic motion, in which centrifugal dynamics are neglected and slippage is due only to steering. Interestingly, it has been demonstrated that in order to achieve stability with fast motion (i.e., with some slippage contributed by centrifugal forces), it must be guaranteed that  $y_{ICRv}$  is bounded [13].

From Eqs.(2)-(5), the kinematic relation (1) can be obtained as :

$$\begin{pmatrix} v_x \\ v_y \\ \omega_z \end{pmatrix} = A \cdot \begin{pmatrix} V_l \\ V_r \end{pmatrix} \quad (6)$$

where the elements of matrix  $A$  only depend on tread ICR coordinates and correction factors:

$$A = \frac{1}{x_{ICRr} - x_{ICRl}} \cdot \begin{bmatrix} -y_{ICRv} \cdot \alpha_l & y_{ICRv} \cdot \alpha_r \\ x_{ICRr} \cdot \alpha_l & -x_{ICRl} \cdot \alpha_r \\ -\alpha_l & \alpha_r \end{bmatrix}. \quad (7)$$

Note that in the case of an ideal symmetrical kinematic model (i.e., ICRs lie symmetrically on the local  $X$  axis and  $y_{ICRv} = 0$ ), matrix  $A$  takes the following form:

$$A = \frac{\alpha}{2x_{ICR}} \cdot \begin{bmatrix} 0 & 0 \\ x_{ICR} & x_{ICR} \\ -1 & 1 \end{bmatrix} \quad (8)$$

where  $\alpha = \alpha_l = \alpha_r$  and  $x_{ICR} = -x_{ICRl} = x_{ICRr}$ .

Besides, this locomotion system introduces a non-holonomic restriction in the motion plane because the non-square matrix  $A$  has no inverse.

It must be noted that the above expressions also represent kinematics for ideal wheeled differential drive vehicles, as illustrated by Fig. 3. Therefore, for instantaneous motion, kinematic equivalences can be considered between skid-steer and ideal wheel vehicles.

The difference between both traction schemes is that whereas ICRs for single ideal wheels are constant and coincident with the ground contact points, tread ICRs are dynamics-dependent and always lie outside of the tread centerlines because of slippage. Thus, less slippage results in tread ICRs that are closer to the vehicle.

Significantly, the center of mass of a vehicle affects tread ICRs, as illustrated by Fig. 3. If it is closer to one side, then that side's wheels will slip less on account of pressure and its ICR will be closer to the vehicle. Conversely, the opposite tread ICR will be farther. Furthermore, the area of the contact patch and its distribution also affect tread ICRs. Thus, if the center of mass is closer to the front or rear ends of the vehicle, pressure distribution concentrates onto a portion of the tread contact surface, which results in closer tread ICRs and a displacement of the  $y_{ICRv}$  coordinate. In this sense, tire pressure also affects ICR positions. These effects can be quantified by stating appropriate indexes.

A steering efficiency index  $\chi$  of the vehicle can be defined as the inverse of the normalized distance between the tread

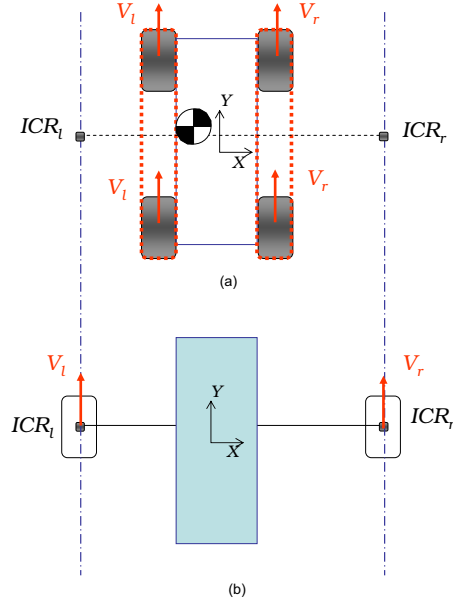


Fig. 3. Kinematic equivalence between the tread ICRs of a skid-steer vehicle (a) and wheel contact points of an ideal differential drive vehicle (b).

ICRs:

$$\chi = \frac{L}{x_{ICRr} - x_{ICRl}}, \quad (0 < \chi \leq 1) \quad (9)$$

where  $L$  is the distance between tread centerlines. Index  $\chi$  is equal to 1 when no slippage occurs (i.e., ideal differential drive). Besides, a normalized eccentricity index can be defined as follows:

$$e = \frac{x_{ICRr} + x_{ICRl}}{x_{ICRr} - x_{ICRl}} \quad (10)$$

which is equal to 0 when tread ICRs are symmetrical with respect to the local  $Y$  axis.

The major consequence of the study above is that the effect of vehicle dynamics is introduced in the kinematic model just by two points in local coordinates:  $ICR_l$  and  $ICR_r$ . These points are bounded variables for skid-steer vehicles and coincide with wheel contact points for ideal differential drive.

### III. EXPERIMENTAL KINEMATICS IDENTIFICATION

A simple experiment, first proposed in [16], can be used to derive a symmetric kinematic model. When equal opposite tread speed control inputs  $V_r$  and  $V_l$  are issued, the vehicle exhibits an approximately pure rotation about its  $Z$ -axis. Then, the following equation can be applied:

$$x_{ICR} \approx \frac{\int V_r dt - \int V_l dt}{2 \cdot \phi}, \quad (11)$$

where  $\phi$  represents the actual rotated angle. Similarly, the value  $\alpha$  can be adjusted by measuring the actual traveled distance  $d$  in straight motion:

$$\alpha \approx \frac{2d}{\int V_r dt + \int V_l dt}. \quad (12)$$

This simple procedure offers a kinematic solution that accounts for wheel slippage. However, it does not contemplate neither the asymmetric effects of the center of mass nor mechanical misalignments.

Therefore, a more exhaustive experimental setup is proposed in order to obtain the complete kinematic relation expressed by (7). In this case, the parameter identification method comprises two steps [17]. The first is to obtain experimental data from both external and internal sensors. Then, an optimization tool is employed to find the parameter values that best fit the data. Optimization is required, since actual tread ICR positions vary during navigation on account of dynamics.

Genetic algorithms (GAs) are proposed as an appropriate search method for this problem. This is a derivative-free stochastic optimization tool, where each point in a solution space is encoded into a bit string (chromosome) and is associated with a fitness value. Starting from an initial random population, points with better fitness values are used to construct a new population of solutions by means of genetic operators. Thus, after several iterations (generations), the overall fitness value is improved.

GAs are useful for finding optimized values for the set of kinematic parameters  $\mathbf{K} = \{x_{ICRl}, x_{ICRr}, y_{ICRv}, \alpha_r, \alpha_l\}$  from experimental data because no significant a priori knowledge exists about them, it is straightforward to code them as bit strings, and a fitness value can be assigned to new solutions. Note that the number of parameters is one less than the number of elements in matrix  $A$ .

Data collection experiments consist of several representative paths on a particular soil type, with diverse rotational and translational speeds and accelerations. Data logged from internal readings (e.g., shaft encoders or inertial sensors) are needed to replay odometric estimations according to alternative kinematic parameters. External sensor readings (e.g., from a laser scanner or Differential GPS) occur at a lower rate, and are necessary to accurately determine the actual motion of the vehicle. Thus, training paths can be broken into a number  $N$  of short segments according to the external sensor rate. This way, each segment contains several consecutive internal readings in order to estimate a kinematic pose increment  $(\Delta\hat{x}, \Delta\hat{y}, \Delta\hat{\phi})$  by integrating (6) with (7), as well as an accurate motion increment  $(\Delta x, \Delta y, \Delta\phi)$  calculated from external readings. Fitness of the alternative solutions evaluated by the GA can be assessed as the sum of the squared odometric errors for the  $N$  recorded segments:

$$J(\mathbf{K}) = \sum_{i=1}^N \left( (\Delta x_i - \Delta\hat{x}_i)^2 + (\Delta y_i - \Delta\hat{y}_i)^2 + (\Delta\phi_i - \Delta\hat{\phi}_i)^2 \right). \quad (13)$$

At each GA iteration, a set of solutions with better overall errors is chosen for computing a new population with

the crossover and mutation operators. As a result, constant kinematic parameters can be optimized off-line for a specific robotic task, according to typical path motions, particular soil types, and speed ranges.

#### IV. CASE STUDY: APPLICATION TO THE P3-AT ROBOT

##### A. The Pioneer P3-AT robot

The P3-AT has a 4-wheel drive skid-steer platform. It measures approximately 0.5 m in length and is 0.25 m tall. Tread length (i.e., the distance between the front and rear wheels) is 0.27 m. Two different wheels sets are provided by the manufacturer: Solid rubber tires of 19 cm diameter (intended mainly for indoor use), and pneumatic tires of 22 cm diameter (see Fig. 4). The distance between longitudinal tread centerlines is  $L = 0.4$  m for both tire types. The drive systems use reversible-DC motors equipped with an optical quadrature shaft encoder. It has a maximum speed of 1 wheel revolution per second. The robot weighs 23.6 kg and can carry a 35 kg payload. It can run over two hours on three 12 V DC batteries.



Fig. 4. Two tire types for the robot.



Fig. 5. DGPS base (foreground right) and P3-AT robot (left).

The robot receives orders from a PC and sends operational information under a built-in client-server architecture. Odometric estimations are calculated from an implicit symmetric kinematic model, which can be adjusted by the user through a pair of integer parameters, namely *Ticksmm* and *Revcount*.

### B. Kinematic parametrization

There are two alternative ways to implement approximate kinematics of the P3-AT robot for motion control and dead-reckoning. First, the server incorporates a symmetric model, as in (8), that can be specified through the *Ticksmm* and *Revcount* parameters. Secondly, an asymmetric model (7) can be implemented on the client by directly processing tick counts from the encoders. Both approaches are discussed below.

1) *Server model parametrization*: The *Ticksmm* parameter describes the number of encoder ticks per millimeter. It depends on wheel radius  $r$ , expressed in millimeters, and is affected by the correction factor  $\alpha$ :

$$Ticksmm = \text{round} \left( \alpha \cdot r \cdot \frac{138}{110} \right), \quad (14)$$

where 138/110 is a constant value that depends on encoders and transmission gears. Besides, *Revcount* represents the number of ticks for a complete revolution of the robot turning in place, which depends on slippage:

$$Revcount = \text{round} \left( \frac{2\pi \cdot x_{ICR} \cdot Ticksmm}{8} \right), \quad (15)$$

where the denominator scales the binary range of the integer.

The factory values for these parameters yield a default symmetric kinematic model with  $\alpha = 1$  and  $x_{ICR} = 0.3$  m (assumed for the pneumatic tires). Note that a non-slip model would have  $x_{ICR} = 0.2$  m.

2) *Client model implementation*: The server does not provide the means to specify the complete asymmetric model, so it has to be implemented on the client PC. Dead reckoning can be computed as (6) with (7) by estimating  $V_r$  and  $V_l$  from tick counts read from the server.

As for motion control, the client has to compute the driver velocities (in mm/s) that are to be sent to the robot with the *setvel2*( $V_l$ ,  $V_r$ ) command. Control inputs can be obtained from (3) and (4) as:

$$V_l = \frac{v_y + x_{ICRl} \cdot \omega_z}{\alpha_l} \quad (16)$$

$$V_r = \frac{v_y + x_{ICRr} \cdot \omega_z}{\alpha_r}, \quad (17)$$

where  $v_x$  references cannot be directly addressed due to the non-holonomic restriction of the locomotion system.

### C. Experimental Identification

The P3-AT has been furnished with a 15.8 kg structure that houses the onboard GPS systems as well as a laptop computer (see Fig. 5). This structure has been considered not to affect the center of gravity of the robot significantly. The onboard Javad GPS receiver provides a precision under 1 cm by accepting RTCM/RTK differential corrections from a nearby GPS base station at a rate of 5 Hz. The portable computer acts as the client in the robotic architecture.

The experiments for kinematic identification have consisted on several joystick controlled paths, where tick counts

	pneumatic (50psi)	pneumatic (20psi)	solid rubber
$y_{ICRv}$	-0.0080	-0.0120	-0.0120
$x_{ICRr}$	0.2998	0.3071	0.2588
$x_{ICRl}$	-0.2758	-0.2553	-0.2667
$\alpha_r$	0.9253	0.9049	0.9128
$\alpha_l$	0.9464	0.9271	0.9047
$\chi$	0.6949	0.7112	0.7612
$e$	0.0417	0.0921	-0.0150

TABLE I

ESTIMATED KINEMATIC PARAMETERS AND INDEXES FOR ASPHALT.

	pneumatic (50psi)	pneumatic (20psi)	solid rubber
$y_{ICRv}$	-0.0159	-0.0128	-0.0139
$x_{ICRr}$	0.2758	0.2899	0.2703
$x_{ICRl}$	-0.2878	-0.2772	-0.2659
$\alpha_r$	0.9418	0.9183	0.9139
$\alpha_l$	0.9457	0.9222	0.9047
$\chi$	0.7098	0.7053	0.7460
$e$	-0.0213	0.0224	0.0082

TABLE II

ESTIMATED KINEMATIC PARAMETERS AND INDEXES FOR SMOOTH CONCRETE.

have been recorded every 10 ms. Each parameter has been coded as an 8 bit string, yielding 40 bit chromosomes for the GA search. Tables I and II present kinematic parameters obtained for asphalt and smooth concrete flat terrains, respectively. In each case, three different wheel configurations have been considered: pneumatic tires at 20 psi (nominal value) and 50 psi (maximum pressure), and solid rubber. Steering efficiency and eccentricity indexes have also been computed.

Independently of terrain and wheel configurations,  $y_{ICRv}$  is always about 1 cm behind of the frame origin, which confirms that it only depends on the center of mass. The loss of thrust power while turning is greater in asphalt than in concrete due to greater friction. This can be observed as a lower steering efficiency value  $\chi$ . In this sense, compact wheels provide better efficiency than pneumatic tires (but less traction). Note also that the  $\alpha$  values are closer to 1 for 50 psi than for 20 psi because the effective wheel radius is closer to the nominal value. The results also show no significant asymmetry with respect to the longitudinal axis  $Y$ , since the eccentricity values are always very close to zero.

### D. Dead-reckoning validation

Validation experiments have been carried out for the six navigation conditions discussed above. Fig. 6 shows a representative example path as estimated by three alternative kinematic models: the default P3-AT symmetric model, an experimental symmetrical model for asphalt and 20 psi pneumatic tires ( $\alpha = 0.91$  and  $x_{ICR} = 0.275$  m) obtained from (11) and (12), and the corresponding optimized asymmetric model. The ICR-based model clearly improves dead-reckoning as compared with accurate path positions provided by the DGPS. Mean squared performance values obtained from all segments in the validation path are shown in Table III.



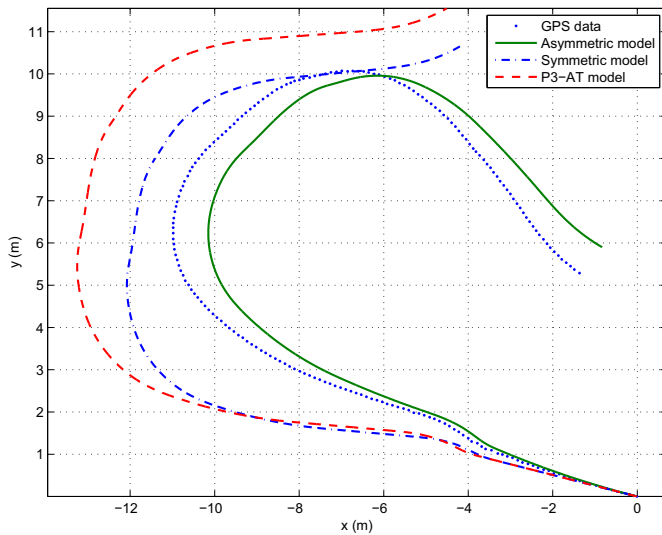


Fig. 6. Validation path for asphalt and 20 psi pneumatic tires.

	Asymmetric	P3-AT	Symmetric
mean squared $\Delta x$ error	0.00010	0.00183	0.00162
mean squared $\Delta y$ error	0.00011	0.00468	0.00455
mean squared $\Delta \phi$ error	0.0359	0.0359	0.0359
mean squared $J$ error	0.0361	0.0424	0.0421

TABLE III

MEAN PERFORMANCE VALUES FOR ALL SEGMENTS IN THE VALIDATION PATH.

## V. CONCLUSIONS

The paper proposes a method for improving real-time motion control and dead-reckoning of wheeled skid-steer vehicles without introducing the complexity of dynamics computations in the loop. The method experimentally derives an approximate kinematic model based on the boundedness of the Instantaneous Centers of Rotation of both treads on the motion plane. The model relates drive and vehicle velocities by considering the effects of slippage. Moreover, it incorporates fine-tuning parameters for misalignments and other hidden mechanical inaccuracies.

The major contributions of the paper are the following:

- The geometric analogy with an ideal differential drive model provides a physical interpretation to the coefficients of the kinematic matrix presented by [8].
- An easy to reproduce experimental method based on external sensor motion estimation and Genetic Algorithms to identify an approximate kinematic model for wheeled skid-steer vehicles.
- A kinematic analysis of the Pioneer P3-AT robot. Configuration parameters of manufacturer's implicit kinematic model have been related to the proposed method.
- Analysis of experimental dead reckoning results from the application of the experimental model with different wheel and terrain configurations.

For future work, it would be interesting to integrate this enhanced kinematic model with inertial measurements for irregular terrains.

## ACKNOWLEDGMENTS

This work was partially supported by the Spanish CICYT projects DPI 2005-01391 and DPI 2005-00207.

## REFERENCES

- [1] L. Champeny-Bares, S. Coppersmith, and K. Dowling, "The Terregator mobile robot," Carnegie Mellon University, Pittsburgh, Pennsylvania, Tech. Rep. CMU-RI-TR-93-03, 1991.
- [2] B. Shamah, M. D. Wagner, S. Moorehead, J. Teza, D. Wettergreen, and W. Whittaker, "Steering and control of a passively articulated robot," in *SPIE Sensor Fusion and Decentralized Control in Robotics Systems IV*, 2001.
- [3] K. Wedeward, S. Bruder, V. Yodaiken, and J. Guilberto, "Low-cost outdoor mobile robot: a platform for landmine detection," in *Proc. IEEE 42nd Midwest Symposium on Circuits and Systems*, 1999, pp. 131–134.
- [4] A. Chetchetka, S. Hughes, R. Glington, M. Koes, M. Lewis, I. Nourbakhsh, D. Rosenberg, K. Sycara, and J. Wang, "Robocup rescue robot league team raptor (USA)," in *Proc. RoboCup US Open 2005 Rescue Robot League Competition*, Atlanta, Georgia, USA, 2005.
- [5] *Pioneer 3 and Pioneer 2 H8-Series Operations Manual, version 3*, ActivMedia Robotics, LLC, Amherst, NH, August 2003.
- [6] J. Y. Wong and W. Huang, "Wheels vs. tracks: A fundamental evaluation from the traction perspective," *Journal of Terramechanics*, vol. 43, pp. 27–42, 2006.
- [7] H. Chung, L. Ojeda, and J. Borenstein, "Accurate mobile robot dead-reckoning with a precision-calibrated fiber-optic gyroscope," *IEEE Transactions on Robotics and Automation*, vol. 17, no. 1, pp. 329–336, 2001.
- [8] G. Anousaki and K. J. Kyriakopoulos, "A dead-reckoning scheme for skid steered vehicles in outdoor environments," in *Proc. IEEE Int. Conf. on Robotics and Automation*, New Orleans, LA, 2004, pp. 580–585.
- [9] Z. Fan, J. Borenstein, D. Wehe, and Y. Koren, "Experimental evaluation of an encoder trailer for dead-reckoning in tracked mobile robots," in *Proc. of the IEEE International Symposium on Intelligent Control*, Monterey, CA, 1995, pp. 571–576.
- [10] L. Caracciolo, A. D. Luca, and S. Iannitti, "Trajectory tracking control of a four-wheel differentially driven mobile robot," in *Proc. of the IEEE Int. Conf. on Robotics and Automation*, Detroit, USA, 1999, pp. 2632–2638.
- [11] K. Kozłowski and D. Pazderski, "Modelling and control of a 4-wheel skid-steering mobile robot," *Int. J. Appl. Math. Comput. Sci.*, vol. 14, no. 4, pp. 477–496, 2004.
- [12] E. Maalouf, M. Saad, and H. Saliah, "A higher level path tracking controller for a four-wheel differentially steered mobile robot," *Robotics and Autonomous Systems*, vol. 54, pp. 23–33, 2006.
- [13] K. Kozłowski and D. Pazderski, "Practical stabilization of a skid-steering mobile robot - a kinematic-based approach," in *Proc. of the IEEE 3rd International Conference on Mechatronics*, Budapest, Hungary, 2006, pp. 519–524.
- [14] A. Le, D. Rye, and H. F. Durrant-Whyte, "Estimation of track-soil interactions for autonomous tracked vehicles," in *Proc. of the IEEE Int. Conf. on Robotics and Automation*, vol. 2, Albuquerque, USA, 1997, pp. 1388–1393.
- [15] J. Yi, D. Song, J. Zhang, and Z. Goodwin, "Adaptive trajectory tracking control of skid-steered mobile robots," in *Proc. IEEE International Conference on Robotics and Automation*, Rome, Italy, 2007, pp. 2605–2610.
- [16] S. Pedraza, R. Fernández, V. Muñoz, and A. García-Cerezo, "A motion control approach for a tracked mobile robot," in *Proc. of the 4th IFAC International Symposium on Intelligent Components and Instruments for Control Applications*, Buenos Aires, Argentina, 2000, pp. 147–152.
- [17] J. L. Martínez, A. Mandow, J. Morales, S. Pedraza, and A. García-Cerezo, "Aproximating kinematics for tracked mobile robots," *The International Journal of Robotics Research*, vol. 24, no. 10, pp. 867–878, 2005.
- [18] L. Ojeda and J. Borenstein, "Reduction of odometry errors in over-constrained mobile robots," in *Proc. of the UGV Technology Conference at the 2003 SPIE AeroSense Symposium*, Orlando, FL, 2003.